NANO LETTERS

pubs.acs.org/NanoLett Letter

Tailoring Topological Transitions of Anisotropic Polaritons by Interface Engineering in Biaxial Crystals

Yali Zeng,[○] Qingdong Ou,[○] Lu Liu, Chunqi Zheng, Ziyu Wang, Youning Gong, Xiang Liang, Yupeng Zhang, Guangwei Hu, Zhilin Yang, Cheng-Wei Qiu, Qiaoliang Bao,* Huanyang Chen,* and Zhigao Dai*

Cite This: https://doi.org/10.1021/acs.nanolett.2c00399 Read Online

ACCESS | Metrics & More | Article Recommendations | Supporting Information

ABSTRACT: Polaritons in polar biaxial crystals with extreme anisotropy offer a promising route to manipulate nanoscale light−matter interactions. The dynamic modulation of their dispersion is of great significance for future integrated nano-optics but remains challenging. Here, we report tunable topological transitions in biaxial crystals enabled by interface engineering. We theoretically demonstrate such tailored polaritons at the interface of heterostructures between graphene and α-phase molybdenum trioxide (α-MoO_3). The interlayer coupling can be modulated by both the stack of graphene and α-MoO_3 and the magnitude of the Fermi level in graphene enabling a dynamic topological transition. More interestingly, we found that the wavefront transition occurs at a constant Fermi level when the thickness of α-MoO_3 is tuned. Furthermore, we also experimentally verify the hybrid polaritons in the graphene/α-MoO_3 heterostructure with different thicknesses of α-MoO_3. The interface engineering offers new insights into optical topological transitions, which may shed new light on programmable polaritonics, energy transfer, and neuromorphic photonics.

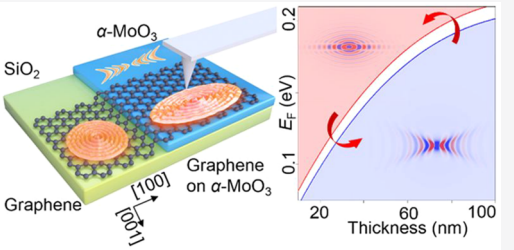

KEYWORDS: *Topological transitions, Anisotropic polaritons, Biaxial crystal, Dispersion engineering, Active tuning*

INTRODUCTION

Polaritons—hybrid quasi-particles with photons—provide a unique way to harness and manipulate light on the nanoscale due to the strong light−matter interaction. Conventional surface plasmon polaritons (PPs) propagating along the interface of a metal and a dielectric have been widely studied with intrinsic electronic scattering and plasmonic loss.[1−7] The emergent polaritons in van der Waals (vdW) materials feature a low loss and ultrahigh confinement, including PPs in graphene[8−10] and black phosphorus (BP),[11,12] phonon polaritons (PhPs) in hexagonal boron nitride (hBN)[13−15] and α-phase molybdenum oxide (α-MoO_3),[16−19] and exciton polaritons in transition-metal dichalcogenides,[20−22] showing promise for their use in integrated and ultrathin nanophotonic devices. This great promise relies on their controllable propagation characteristics as dominated by the dispersion of polaritons. For instance, polaritons in biaxial crystals[23−26] have a direction-related momentum, exhibiting interesting and distinctive nano-optical phenomena, such as highly directional propagation, topological transitions (TTs),[27] and canalization.[28] Recently, there has been widespread interest in studying the polaritons at the interface between biaxial crystals and a dielectric background,[29] since it offers direct access and manipulation of the wave at the surface. Such responses can also be divided into in-plane or out-of-plane responses, depending on the distinguishability of propagation characteristics along different directions at the interface. An example is that polaritons at the top surface of exfoliated hBN or graphene are in-plane isotropic with a circular wavefront, but patterning them into artificially biaxial metasurfaces with periodic array of nanoribbons can induce in-plane anisotropy and even a hyperbolic to elliptic TT.[30−33] Furthermore, one can stack naturally biaxial crystals such as α-MoO_3 thin flakes and manipulate the interlayer coupling via their twisted angle to stimulate such TTs.[34−37] Those tailorable polaritons have represented an important step toward the on-demand control of polaritons.

Biaxial crystal heterostructures provide another promising route to engineer the dispersion of polaritons. To configure the in-plane anisotropy of PhPs in hBN, stacking of hBN onto anisotropic BP has been proven to induce an in-plane ellipticity of PhP dispersions.[38] Through anisotropy-oriented mode couplings and TT, the in-plane hyperbolic response of PhPs has been controlled and switched at the heterostructural

Received: February 2, 2022
Revised: April 14, 2022

https://doi.org/10.1021/acs.nanolett.2c00399
Nano Lett. XXXX, XXX, XXX−XXX

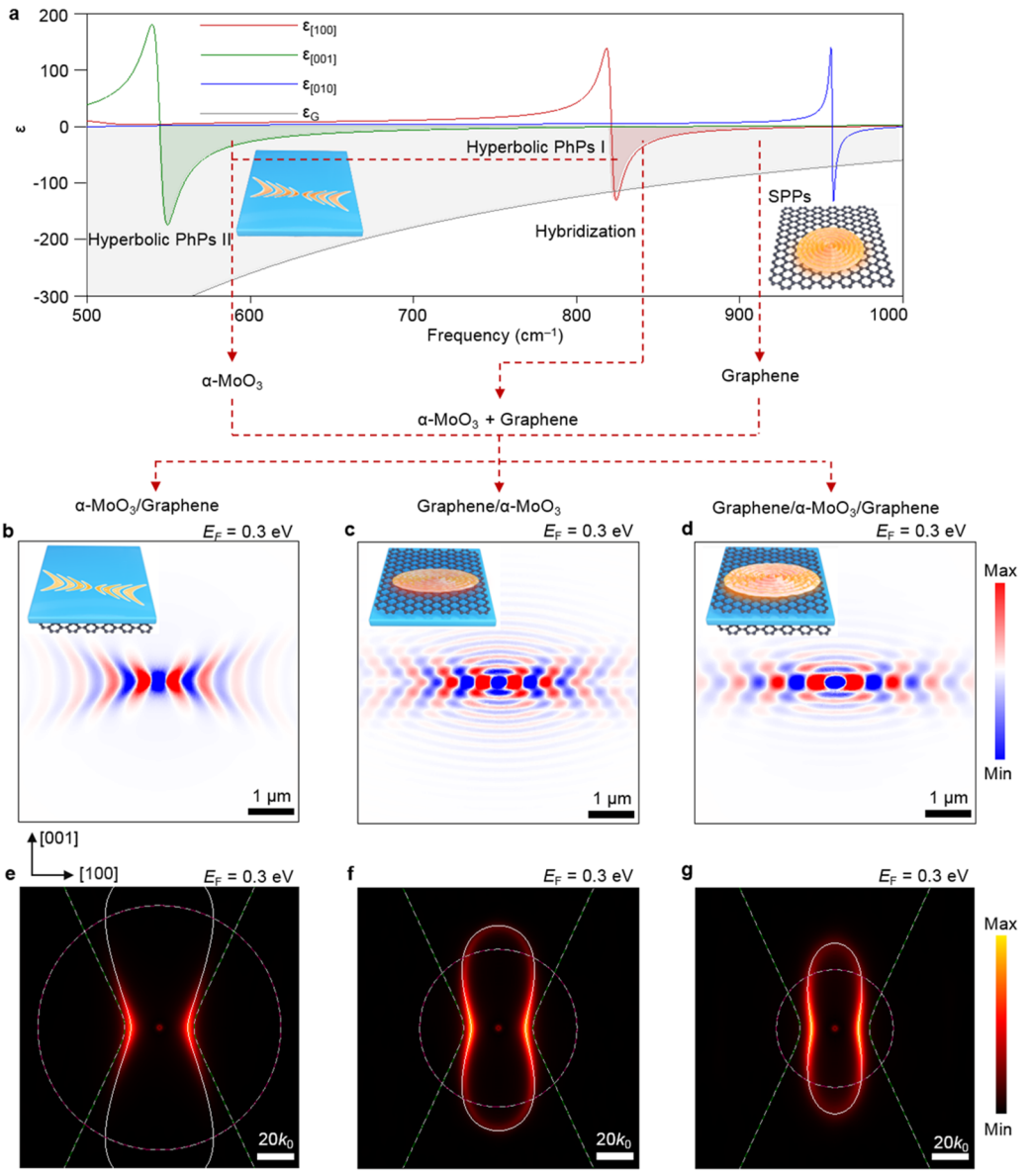

Figure 1. Stack-dependent topological transitions of polaritons in α-MoO_3 and graphene heterostructures via interface engineering. (a) Real parts of the permittivity of α-MoO_3 along the three principal axes and graphene. The green and red regions denote the Reststrahlen bands I and II of α-MoO_3, respectively. The light gray region represents the band where the SPPs can be excited in graphene. (b−d) Simulated field distributions Re(E_z) of hybrid plasmon−phonon polaritons propagating in the α-MoO_3/graphene, graphene/α-MoO_3, and graphene/α-MoO_3/graphene heterostructure and (e−g) the corresponding dispersions (fast Fourier transform (FFT) and analytical isofrequency curve) at a frequency of 905 cm^{-1}, respectively. The white solid curves denote the calculated dispersion bands of heterostructures at low k. The green and red dashed curves correspond to the dispersion curves of the graphene with different stacks and α-MoO_3 on the substrate, respectively. The thickness of α-MoO_3 is 100 nm.

interfaces between α-MoO_3 and SiC, enabling the propagation of hyperbolic PhPs along originally forbidden directions.[39,40] These examples offer further approaches to modulate the dispersion of polaritons. However, all of these engineering tools lack dynamic tunability. The active tuning of anisotropic polaritons and their TTs is highly desired for integrated photonic circuits but remains unexplored.

In this work, we show tunable TTs in biaxial crystals enabled by interface engineering. With the natural biaxial crystal α-MoO_3 and isotropic graphene, we demonstrate tunable polaritons at the interface of graphene and α-MoO_3, especially for the TT of hybrid polaritons. In this hybrid system, we theoretically predict that the tailored interlayer coupling enables control of the TT of polariton dispersions and experimentally demonstrate the hybrid polaritons at the heterostructural interfaces by real-space nanoimaging. Due to the tunability of Fermi levels in graphene, the approach appears as a new strategy to dynamically adjust the interlayer coupling to achieve the manipulation of optical TTs. Moreover, tuning of the thickness of the α-MoO_3 slab and thereby the hyperbolic PhP dispersions could be another dimension for the control of anisotropic polaritons.

RESULTS AND DISCUSSION

Due to their intrinsic anisotropy, biaxial crystals can support in-plane elliptical and hyperbolic polaritons according to the signs of the in-plane permittivity tensors. To tailor the in-plane

https://doi.org/10.1021/acs.nanolett.2c00399
Nano Lett. XXXX, XXX, XXX−XXX

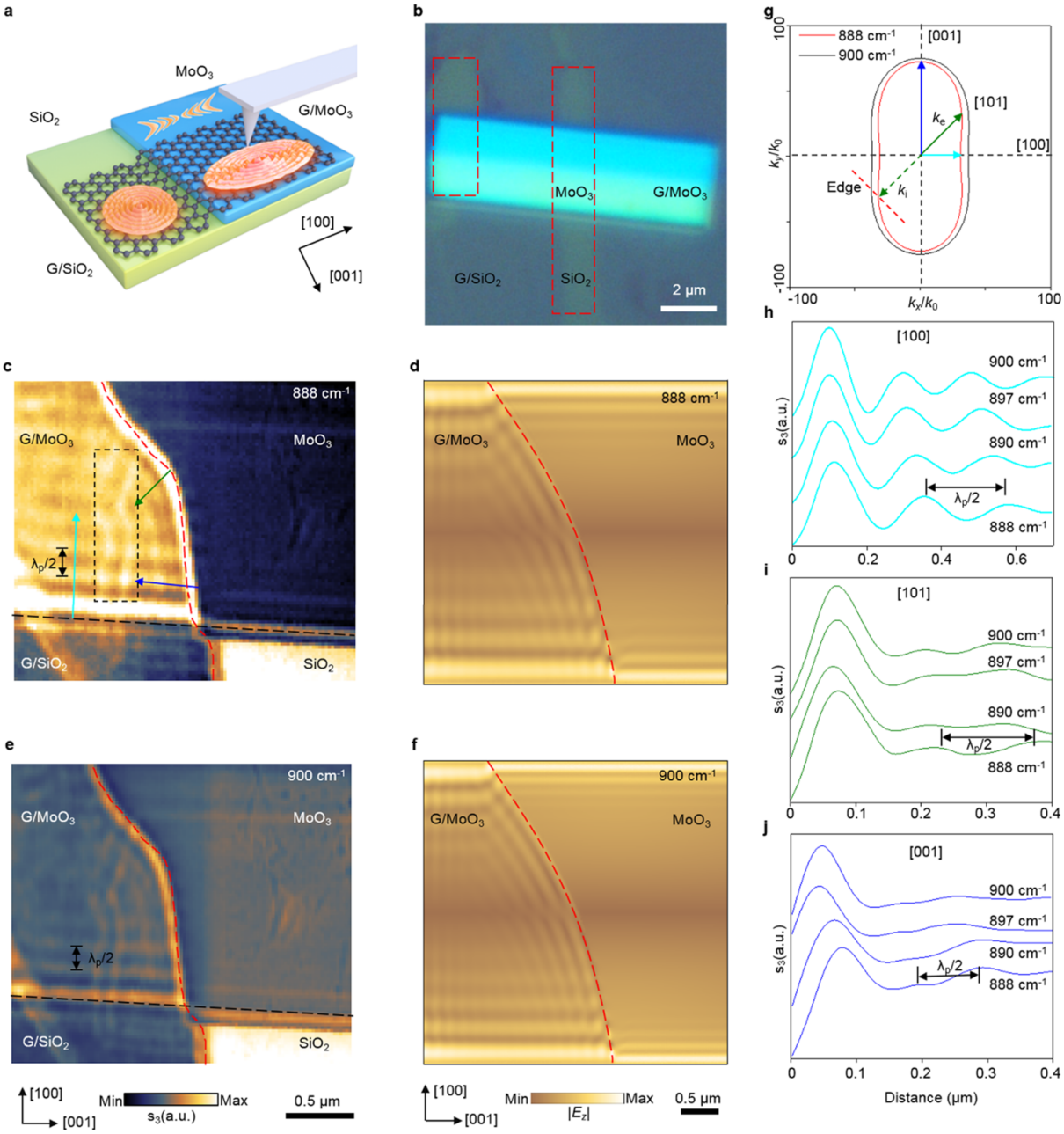

Figure 2. Real-space imaging of topological transitions in the graphene/α-MoO_3 heterostructure. (a) Schematic of the s-SNOM experimental scheme. (b) Optical image of the graphene/α-MoO_3 heterostructure. Experimental near-field amplitudes $s(\omega)$ (c, e) and simulated field (d, f) distributions at a frequency of 888 and 900 cm^{-1}, respectively. (g) Isofrequency contours of hybrid polaritons in graphene/α-MoO_3 at 888 cm^{-1} (black curve) and 900 cm^{-1} (purple curve). (h–j) Line plots of measured hybrid polaritons along the cyan, green, and blue lines in Figure 2c at different frequencies. The thickness of α-MoO_3 is 25 nm, and the Fermi level of graphene is 0.2 eV.

polariton dispersions, we selected graphene as a tunable extra polariton source due to its flexible tunability and ease of fabrication and stacking and the biaxial crystal α-MoO_3 to study the interlayer coupling for tailoring TTs of anisotropic polaritons. To directly show the overlapping dielectric responses, the real parts of the permittivity tensors of graphene (see Methods in the Supporting Information) and α-MoO_3 along the three principal axes[17] are plotted in Figure 1a, suggesting the potential formation of hybrid plasmon–phonon polaritons mode in two excitation bands (Figure 1a, 545–820 and 851–972 cm^{-1}). Three configurations were proposed to fully engineer the interface of graphene/α-MoO_3 heterostructures (see the insets in Figure 1b–d): an α-MoO_3/graphene heterostructure (MoO_3/G), a graphene/α-MoO_3 heterostructure (G/MoO_3), and a graphene/α-MoO_3/graphene sandwich heterostructure (G/MoO_3/G), all with SiO_2/Si substrates. The simulated field distribution Re(E_z) for the MoO_3/G heterostructure is shown in Figure 1b, exhibiting hybrid plasmon–phonon polaritons with an evident concave wavefront. Here, the Femi level of graphene is E_F = 0.3 eV. The corresponding in-plane dispersion of the hyperbolic hybrid polaritons can be viewed more intuitively by the fast Fourier transform (FFT) of Re(E_z) (Figure 1e), which is in excellent agreement with the analytical dispersion curve (white solid curve). In contrast, with the same Fermi level, hybrid polaritons in the G/MoO_3 heterostructure

https://doi.org/10.1021/acs.nanolett.2c00399
Nano Lett. XXXX, XXX, XXX–XXX

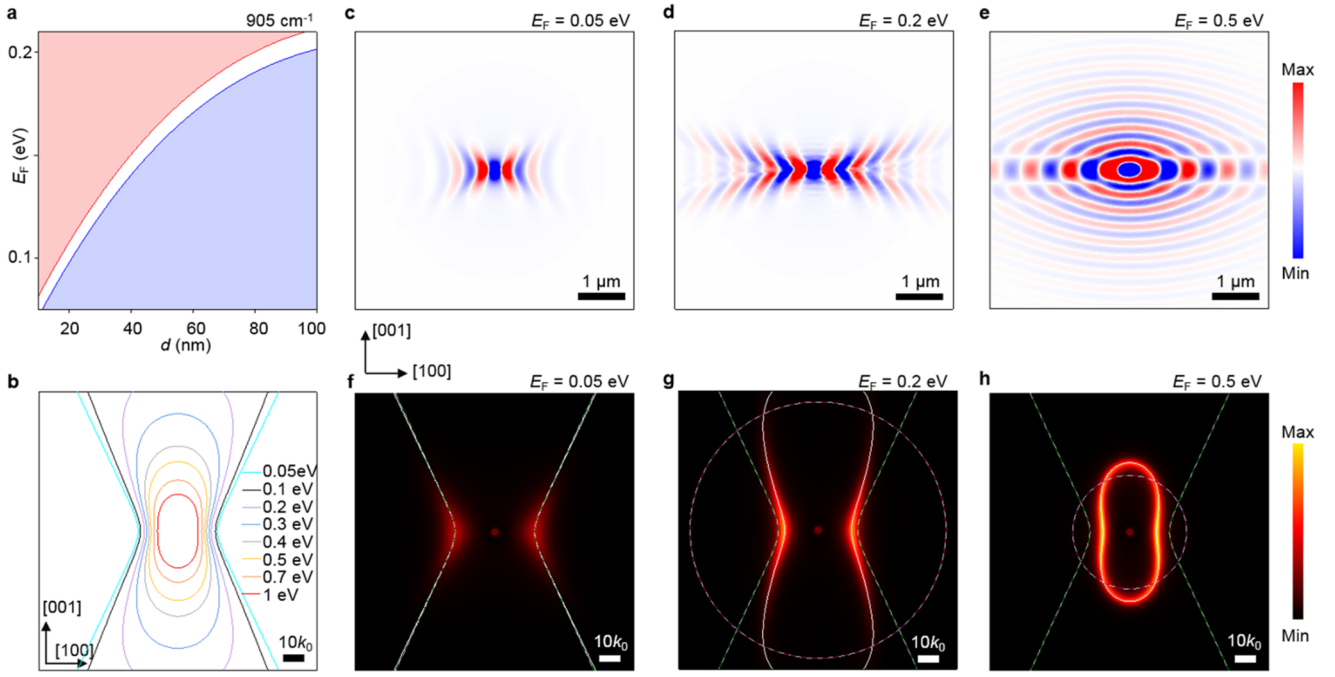

Figure 3. Tunable hybrid plasmon−phonon polaritons in graphene/α-MoO_3 heterostructures. (a) Relationship between the Fermi level required for a wavefront transition at 905 cm^{-1} and the thickness of α-MoO_3. (b) Isofrequency curves for the hybrid polaritons in the graphene/α-MoO_3 heterostructure with different Fermi levels in graphene at 905 cm^{-1}. The heterostructure is stacked on a SiO_2/Si substrate. (c−e) Simulated field distributions Re(E_z) and (f−h) the corresponding FFT images of hybrid plasmon−phonon polaritons in graphene/α-MoO_3 heterostructures. The white solid curves denote the calculated dispersion bands of heterostructures. The green and red dashed curves correspond to the dispersion curves of graphene with different Fermi levels and α-MoO_3 on the substrate, respectively. The thickness of α-MoO_3 is 100 nm.

(Figure 1c) show a distinct closed wavefront, indicating finite and direction-dependent in-plane wavevectors (Figure 1f). For the G/MoO_3/G sandwich heterostructure (Figure 1d), a closed dispersion contour is also obtained (Figure 1g), but with a smaller cutoff of in-plane wavevector in comparison to Figure 1f. Due to the SiO_2/Si substrate with broken symmetry in the z direction, the graphene SPPs with different momentums are excited in three heterostuctures (the red dashed curves in Figure 1e−g), resulting in different coupled hybrid polaritons. Furthermore, to exclude the substrate effect, the field distributions and corresponding dispersions of suspended heterostructures have also been simulated (Figure S9), indicating no difference in the suspended G/MoO_3 and MoO_3/G heterostructures. Those results are very interesting, as they suggest the importance of the stack when we break the symmetry of the superstrate and substrate.

We now experimentally verify the TTs of hybrid plasmon−phonon polaritons. The G/MoO_3 heterostructures were fabricated on an SiO_2/Si substrate. A scattering-type near-field optical microscope (s-SNOM) was employed to map the polaritons, as schematically illustrated in Figure 2a. The optical image of the sample is shown in Figure 2b; this sample was prepared by selectively removing graphene (by using oxygen plasma) on top of an α-MoO_3 flake. Figure 2c depicts the near-field amplitude images measured experimentally at a frequency of 888 cm^{-1}. Only horizontal fringes are observed in the region of α-MoO_3,[19] suggesting the in-plane hyperbolic polaritons propagating along the [100] direction. In large contrast, in the region of G/MoO_3, fringes can be observed in both horizontal and vertical directions, which matches well with the simulated field distributions in Figure 2d. Similar phenomena are observed at 900 cm^{-1} in Figure 2e,f but with a smaller fringe spacing. In addition, extra fringes (black dashed rectangles) appear in the data in Figure 2c,e. To explore the origin of extra fringes, we have compared the collocated topography (see Figure S6a) with the SNOM image (Figure S6b). However, it is hard to identify an obvious variation in the thickness or continuity of the film. Therefore, we can exclude the possible causes by wrinkles, cracks, or thicker layers. The extra fringes are most likely correlated with the grain boundary in the graphene film, which normally reflects the polaritons on both sides and gives birth to symmetrical bright fringes in the SNOM image.[41] Remarkably, hybrid polaritons in the G/MoO_3 heterostructure can propagate along both [100] and [001] directions with different fringe spacings, a direct signature that the dispersion of polaritons has transited from an open hyperbola to a closed ellipse. The isofrequency curves of elliptical hybrid polaritons in Figure 2g show direction-dependent in-plane wavevectors, corresponding to different fringe spacings in Figure 2c,e. The in-plane wavevector increases with the angle between the edge and the [001] direction, resulting in reduced polariton wavelengths along the [001] direction.

To quantitatively study the polaritonic features, the line profiles of experimentally measured field distributions in Figure 2c at different frequencies are plotted in Figure 2h−j. The oscillating curves along the [100], [101], and [001] directions reveal the different wavevectors of propagating hybrid polaritons along these three directions, verifying the transformation of hyperbolic polaritons in G/MoO_3. Specifically, the polariton wavelengths λ_p along the [100], [101], and [001] directions at a frequency of 888 cm^{-1} are 0.44, 0.35, and 0.2 μm, respectively, greater than that of PhPs in α-MoO_3 (~0.15 μm).[16] Therefore, the wavelengths and wavevectors of hybrid polaritons can be easily tuned along different directions over a

https://doi.org/10.1021/acs.nanolett.2c00399
Nano Lett. XXXX, XXX, XXX−XXX

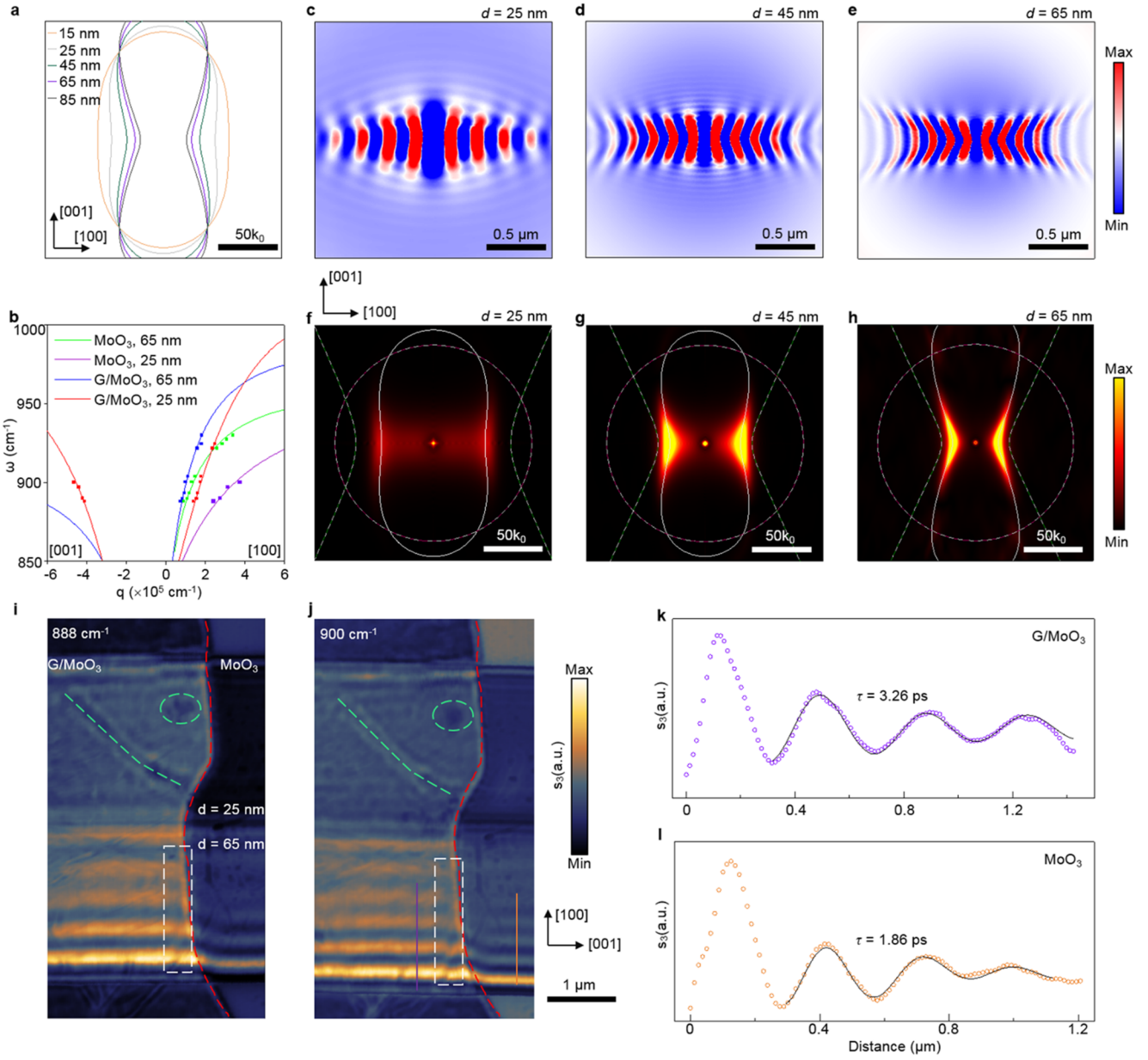

Figure 4. Thickness-dependent hybrid plasmon−phonon polaritons in graphene/α-MoO_3 heterostructures. (a) Isofrequency curves for the hybrid polaritons in the graphene/α-MoO_3 heterostructure with different thicknesses of α-MoO_3 at a frequency of 905 cm^{-1}. The heterostructure is stacked on a SiO_2/Si substrate. (b) Dispersion relations for PhPs and hybrid polaritons in different structures. The solid curves represent the analytical results, and the dots indicate experimental data extracted from s-SNOM. The Fermi level of graphene is 0.2 eV. (c−e) Simulated field distributions Re(E_z) and (f−h) the corresponding FFT images for the graphene/α-MoO_3 heterostructure. The white solid curves denote the calculated dispersion bands of heterostructures. The green and red dashed curves correspond to the dispersion curves of the graphene and α-MoO_3 with different thicknesses on the substrate, respectively. Experimentally measured field distributions at (i) 888 cm^{-1} and (j) 900 cm^{-1}. The Fermi level of graphene is 0.2 eV. Line plots of measured hybrid polaritons along the (k) purple line and (l) orange line in (j). The dots are the measured data, and the solid curves are the fittings.

wide spectral range by just slightly changing the excitation frequency.

Graphene SPPs can be tuned by electrical gating and doping.[8−10] The dispersions and wavevectors of PhPs in α-MoO_3 are also sensitive to intercalated ions[18,42,43] and are thickness-dependent.[18] Hyperbolic PhPs in α-MoO_3 can only propagate along certain angle ranges. However, in the G/MoO_3 structure, the SPPs in graphene can propagate along the forbidden direction of hyperbolic PhPs in α-MoO_3 because α-MoO_3 behaves as a dielectric in the [001] direction. Hybrid polaritons formed by the coupling of the SPPs in graphene and the PhPs of α-MoO_3 can propagate in all directions and have a closed isofrequency curve. When the Fermi level E_F of graphene is small, the momentum of graphene SPPs is large, resulting in a large cutoff wavevector $k_{y,cutoff}$ and a large peanut-shaped isofrequency curve of hybrid polaritons. Polaritons with high k have a small wavelength and large damping, which is hard to excite due to the mismatched momentum of air and the G/MoO_3 structure. As the Fermi level increases, the cutoff wavevector $k_{y,cutoff}$ of hybrid polaritons decreases, generating matching polaritons propagating in the [001] direction and a small peanut-shaped or even elliptical isofrequency curve

https://doi.org/10.1021/acs.nanolett.2c00399
Nano Lett. XXXX, XXX, XXX−XXX

(Figure 3b). Furthermore, it is worth noting that polaritons supported by the hyperbolic materials ideally possess an infinite wavevector k. However, we do note that the presence of material losses will cause hyperbolic dispersion to close at high k.[30] Nevertheless, this remains the hyperbolic dispersion characteristic in the finite momentum range. This is because the high-k modes are very weakly excited and hence can be reasonably neglected.

Furthermore, the wavefront of the field reveals the dispersion characteristics of hybrid polaritons in finite k. To this point, we depict the relationship between the Fermi level required for wavefront transition at 905 cm^{-1} and the thickness of α-MoO_3 in Figure 3a. The white channel represents the range of Fermi levels at which the simulated electric field distributions gradually appear in one to several fringes propagating along the [001] direction. Under this channel, hybrid polaritons can only propagate along certain angle ranges and have a hyperbolic wavefront. Above this channel, hybrid polaritons can propagate in all directions even in the forbidden directions of PhPs in α-MoO_3, exhibiting closed wavefronts. Through this channel we can see obvious transitions from closed to hyperbolic wavefront regimes, which is intrinsically due to the momentum matching of air and the G/MoO_3 structure. With a fixed thickness of α-MoO_3 of 100 nm, as the wavevector of graphene plasmons decreases (i.e., the Fermi level increases), the isofrequency curve of hybrid polaritons changes from a hyperbola to an ellipse (Figure 3b). Specifically, at a low Fermi level (e.g., E_F = 0.05 eV), graphene has very low conductivity and does not even support mid-infrared plasma (Figure S8), resulting in very weak coupling between the plasmons of graphene and the hyperbolic phonon polaritons of α-MoO_3 or even noncoupling. In this case, polaritons in G/MoO_3 exhibit an ideal hyperbolic characteristic (Figure 3c,f). As the Fermi level increases, simulated fields accompanied by horizontal fringes emerge (Figure 3d) and the corresponding dispersion (Figure 3g) have a larger open angle at low k. Finally, the simulated fields form a closed wavefront (Figure 3e) with an elliptical dispersion contour (Figure 3h). The TTs can occur in three heterostructures. In addition, due to the different dielectric environments of graphene in different stacking heterostructures, different graphene SPP modes are excited in three heterostructures with the same Fermi level. Consequently, graphene has different regulatory abilities in three heterogeneous structures for hybrid polaritons. A complete dispersion analysis and simulated field distributions of three heterostructures can be found in Figures S10−S12. We can find that the open to closed wavefront transformation can be clearly observed with an increase in the Fermi level to 0.3, 0.6, and 0.3 eV in the G/MoO_3, MoO_3/G and G/MoO_3/G heterostructures, respectively. The results show that the stack and Fermi level can synergistically tune the anisotropy and TTs of such hybrid polariton systems.

The thickness of biaxial crystals is an important factor for tuning the dispersion of hyperbolic polaritons, which will thus affect the hybrid plasmon−phonon polaritons in G/MoO_3 heterostructures. With the fixed Fermi level E_F = 0.16 eV, the isofrequency curve of the G/MoO_3 heterostructure changes from concave (black curve) to convex (orange curve) along the [100] direction as the thickness decreases at a frequency of 905 cm^{-1}, as presented in Figure 4a. Furthermore, an open to closed wavefront transformation occurs with a decrease in thickness of α-MoO_3 (see Figure 4c−e). For thicknesses of 25 and 45 nm, the hybrid polaritons propagate in all directions with an evident direction-dependent wavelength, as depicted in Figure 4c,d. The corresponding FFT images (Figure 4f,g) exhibit weaker ellipticity due to the strong anisotropy and polariton damping.[28] However, due to the very strong anisotropy the electric field propagates in a certain range of angles in the heterostructure consisting of 65 nm thick α-MoO_3 (Figure 4e). The corresponding FFT and the analytical dispersion in Figure 4h exhibit distinct concave shapes in the [100] direction and have a larger cutoff wavevector in the [001] direction. As the thickness of α-MoO_3 increases in the G/MoO_3 heterostructure, the in-plane wavevector of hyperbolic PhPs will gradually decrease[16] and the wavevector of graphene SPPs remains. The coupling of graphene SPPs (the red dashed curves in Figure 4f−h) and hyperbolic PhPs of α-MoO_3 (the green dashed curves in Figure 4f−h) will result in strong anisotropic hybrid polaritons with concave dispersion characteristics in the propagation direction of hyperbolic PhPs.

To corroborate our theoretical results, we fabricated a G/MoO_3 heterostructure by stacking graphene on top of an α-MoO_3 slab with thickness steps of 65 and 25 nm. The measured field distributions at 888 and 900 cm^{-1} are shown in Figure 4i,j, respectively. In the top left region of the G/MoO_3 heterostructure with d = 25 nm, the point defect (green dashed ellipse) and line defect (green dashed curve) respectively generate elliptical fringe patterns and oblique fringes parallel to the defects, verifying the elliptical dispersion of G/MoO_3 heterostructure. In the bottom-left region of the G/MoO_3 heterostructure with d = 65 nm, the polariton wavelength along the [100] direction is larger than that with d = 25 nm, indicating a smaller wavevector, which is consistent with the results in Figure 4b. In addition, the propagating polaritons decay quickly (white dashed box in Figure 4i,j) due to the large wavevector along the [001] directions (Figure 4b). In the right region, there exist only horizontal fringes, belonging to the hyperbolic PhPs of α-MoO_3. The dispersion relations for the polaritons in four different structures are plotted in Figure 4b. By carefully fitting these curves, we use the Fermi level E_F = 0.2 eV for graphene. The wavevectors of hybrid polaritons along the [001] direction are larger than those along the [100] direction, and the hybrid polaritons in the heterostructure with thinner α-MoO_3 exhibit weaker anisotropy, indicating the thickness tunability of anisotropic polaritons.

The interlayer coupling between graphene and α-MoO_3 can also significantly increase the lifetime of hybrid plasmon−phonon polaritons without the need for complex structural fabrication. Figure 4k,l plots the line scans of measured polariton fields along the purple line and orange line in Figure 4j, respectively. Polariton lifetimes can be calculated by using $\tau = L/v_g$,[19] where L is the propagation length obtained from the fitting curves in Figure 4k,l and v_g is the group velocity derived from the dispersion relations in Figure 4b. Through calculations, we found that the propagation length of hybrid polaritons in the G/MoO_3 heterostructure is longer than that in α-MoO_3. It should be noted that, due to the abrupt thickness change in α-MoO_3, the thick part of G/MoO_3 with limited width can be approximately considered as a cavity due to the reflection by the step. The polaritons in the thicker part of G/MoO_3 heterostructure are then likely to form resonance, resulting in an improved lifetime of the hybrid plasmon−phonon systems. Therefore, although the group velocity $v_g = \partial\omega/\partial q$ of hybrid polaritons (see Figure S7) is larger than that of PhPs in α-MoO_3, the polariton lifetime in the G/MoO_3 heterostructure is calculated to be τ = 3.26 ps, which is 1.75

https://doi.org/10.1021/acs.nanolett.2c00399
Nano Lett. XXXX, XXX, XXX−XXX

times higher than that of PhPs (τ = 1.86 ps) in α-MoO_3 and 2.17 times higher than that of hybrid plasmon−phonon polaritons in the graphene nanoribbon/hBN heterostructure,[44] revealing the ultralow-loss character of hybrid polaritons in the G/MoO_3 heterostructure.

CONCLUSION

In conclusion, we have demonstrated tunable TTs enabled by interface engineering in biaxial crystals. More specifically, we theoretically studied the tailoring of hybrid plasmon−phonon polaritons, especially TTs of hybrid polaritons, by engineering the interface of graphene and α-MoO_3 heterostructures and experimentally demonstrated the hybrid polaritons in G/MoO_3 heterostructures with different thicknesses of α-MoO_3. Systematic calculations show that the transitions can be switched by varying the Fermi level in graphene. As the Fermi level of graphene increases, polaritons undergo a TT from open (hyperbolic) to closed (elliptical) dispersions. Furthermore, we find that the thickness of α-MoO_3 is another dimension of regulation, and the wavefront transitions can be readily achieved with a thin MoO_3 slab in the presence of a lower graphene Fermi level. We have established a phase diagram of the tailored wavefront of hybrid plasmon−phonon polaritons based on the Fermi level of graphene and the thickness of α-MoO_3, which lays a foundation for the construction of electronically tunable polaritonic devices, optical signal processing, or neuromorphic photonic circuits based on low-loss polaritons.

It should be noted that, in the preparation for revisions of our paper, we became aware of other papers reporting the tunable phonon polaritons in graphene-covered α-MoO_3 heterostructures.[45−47] Our work was conducted separately.

ASSOCIATED CONTENT

Supporting Information

The Supporting Information is available free of charge at https://pubs.acs.org/doi/10.1021/acs.nanolett.2c00399.

Derivation of the dispersion relation of hybrid polaritons in interface engineering, schematic of an approximate model of interface engineering of biaxial crystals, momentum-directed polaritons in biaxial crystals, schematic of a non-2D approximate model of interface engineering of biaxial crystals, comparison of 2D approximate and non-2D approximate models, numerical simulations and experimental method, Raman spectrum of the G/MoO_3 heterostructure, topography image and s-SNOM measurements of the G/MoO_3 heterostructure, hybrid polaritons in the undoped G/MoO_3 heterostructures, hybrid polaritons in the three suspended heterostructures, and dynamically tunable hybrid plasmon−phonon polaritons in G/MoO_3, MoO_3/G, and G/MoO_3/G heterostructures (PDF)

AUTHOR INFORMATION

Corresponding Authors

Qiaoliang Bao − *Department of Materials Science and Engineering, and ARC Centre of Excellence in Future Low-Energy Electronics Technologies (FLEET), Monash University, Clayton, Victoria 3800, Australia;* orcid.org/0000-0002-6971-789X; Email: qiaoliang.bao@gmail.com

Huanyang Chen − *Department of Physics, Xiamen University, Xiamen 361005, People's Republic of China;* Email: kenyon@xmu.edu.cn

Zhigao Dai − *Engineering Research Center of Nano-Geomaterials of Ministry of Education, Faculty of Materials Science and Chemistry, China University of Geosciences, Wuhan 430074, People's Republic of China;* orcid.org/0000-0002-3105-4605; Email: daizhigao@cug.edu.cn

Authors

Yali Zeng − *Department of Physics, Xiamen University, Xiamen 361005, People's Republic of China; Department of Electrical and Computer Engineering, National University of Singapore, Singapore 117583, Singapore*

Qingdong Ou − *Department of Materials Science and Engineering, and ARC Centre of Excellence in Future Low-Energy Electronics Technologies (FLEET), Monash University, Clayton, Victoria 3800, Australia;* orcid.org/0000-0003-2161-2543

Lu Liu − *Engineering Research Center of Nano-Geomaterials of Ministry of Education, Faculty of Materials Science and Chemistry, China University of Geosciences, Wuhan 430074, People's Republic of China*

Chunqi Zheng − *Department of Electrical and Computer Engineering, National University of Singapore, Singapore 117583, Singapore*

Ziyu Wang − *Department of Materials Science and Engineering, and ARC Centre of Excellence in Future Low-Energy Electronics Technologies (FLEET), Monash University, Clayton, Victoria 3800, Australia; Institute of Materials Research and Engineering, Agency for Science Technology and Research (A*STAR), Singapore 138634, Singapore*

Youning Gong − *College of Electronics and Information Engineering, Shenzhen University, Shenzhen 518060, People's Republic of China;* orcid.org/0000-0002-8114-8095

Xiang Liang − *School of Energy and Power Engineering, Wuhan University of Technology, Wuhan 430063, People's Republic of China*

Yupeng Zhang − *College of Electronics and Information Engineering, Shenzhen University, Shenzhen 518060, People's Republic of China;* orcid.org/0000-0003-2351-5579

Guangwei Hu − *Department of Electrical and Computer Engineering, National University of Singapore, Singapore 117583, Singapore;* orcid.org/0000-0002-3023-9632

Zhilin Yang − *Department of Physics, Xiamen University, Xiamen 361005, People's Republic of China;* orcid.org/0000-0002-4799-1492

Cheng-Wei Qiu − *Department of Electrical and Computer Engineering, National University of Singapore, Singapore 117583, Singapore;* orcid.org/0000-0002-6605-500X

Complete contact information is available at: https://pubs.acs.org/10.1021/acs.nanolett.2c00399

Author Contributions

○Y.Z. and Q.O. contributed equally to this work.

Author Contributions

Q.B. and H.C. conceived the original concept along with kind discussions with Y.Z., Q.O., and Z.D. Q.B. and H.C. supervised the project. Z.D. carried out the near-field imaging experiments with the help of Q.O. and Z.W. Y.Z. performed the modeling and data analysis with the supervision of H.C. Y.Z. carried out

https://doi.org/10.1021/acs.nanolett.2c00399
Nano Lett. XXXX, XXX, XXX−XXX

the simulations with the help of L.L. Z.W., Q.O., and Z.D. contributed to the material synthesis and sample fabrication. Y.Z., Q.O., L.L., C.Z., G.H., C.-W.Q., Q.B., H.C., and Z.D. participated in data analysis and cowrote the manuscript. All authors edited the paper.

Notes

The authors declare no competing financial interest.

■ ACKNOWLEDGMENTS

We thank Pablo Alonso-González and Alexey Y. Nikitin for kind discussions and Weiliang Ma for help with the sample fabrication. We acknowledge support from the National Natural Science Foundation of China (Nos. 52172162, 11874311, and 92050102), the National Key Research & Development Program (Nos. 2016YFA0201900 and 2020YFA0710100), the Australian Research Council (ARC, CE170100039 and DE220100154), and the China Scholarship Council (No. 202006310049). C.-W.Q. acknowledges financial support from the National Research Foundation, Prime Minister's Office, Singapore, under Competitive Research Program Award NRF-CRP22-2019-0006. C.-W.Q. is also supported by a grant (R-261-518-004-720|A-0005947-16-00) from the Advanced Research and Technology Innovation Centre (ARTIC) in NUS. Z.D. acknowledges support from the Fundamental Research Funds for the Central Universities, China University of Geosciences (Wuhan) (No. 162301202610) and the Natural Science Foundation of Guangdong Province. H.C. acknowledges support from the Fundamental Research Funds for the Central Universities (Grant No. 20720200074). Q.B. and H.C. were also supported by 111 project (B16029). Z.W. acknowledges the support of the Natural Science Foundation of Shandong Province, China (ZR2020QE051). The authors acknowledge the support from Shenzhen Nanshan District Pilotage Team Program (LHTD20170006). This work was performed in part at the Melbourne Centre for Nanofabrication (MCN) in the Victorian Node of the Australian National Fabrication Facility (ANFF).

■ REFERENCES

(1) Dai, Z.; Hu, G.; Ou, Q.; Zhang, L.; Xia, F.; Garcia-Vidal, F. J.; Qiu, C.-W.; Bao, Q. Artificial metaphotonics born naturally in two dimensions. *Chem. Rev.* **2020**, *120* (13), 6197−6246.

(2) Maier, S. A., Surface plasmon polaritons at metal/insulator interfaces. In *Plasmonics: Fundamentals and Applications*; Springer: 2007; pp 21−37.

(3) Raether, H., Surface plasmons on smooth surfaces. In *Surface plasmons on smooth and rough surfaces and on gratings*; Springer: 1988; pp 4−39.

(4) Gramotnev, D. K.; Bozhevolnyi, S. I. Plasmonics beyond the diffraction limit. *Nat. Photonics* **2010**, *4* (2), 83−91.

(5) Atwater, H. A.; Polman, A. Plasmonics for improved photovoltaic devices. *Nat. Mater.* **2010**, 1−11.

(6) Jin, Z.; Janoschka, D.; Deng, J.; Ge, L.; Dreher, P.; Frank, B.; Hu, G.; Ni, J.; Yang, Y.; Li, J.; et al. Phyllotaxis-inspired nanosieves with multiplexed orbital angular momentum. *eLight* **2021**, *1* (1), 1−11.

(7) Boltasseva, A.; Atwater, H. A. Low-loss plasmonic metamaterials. *Science* **2011**, *331* (6015), 290−291.

(8) Chen, J.; Badioli, M.; Alonso-González, P.; Thongrattanasiri, S.; Huth, F.; Osmond, J.; Spasenović, M.; Centeno, A.; Pesquera, A.; Godignon, P.; et al. Optical nano-imaging of gate-tunable graphene plasmons. *Nature* **2012**, *487* (7405), 77−81.

(9) Fei, Z.; Rodin, A.; Andreev, G. O.; Bao, W.; McLeod, A.; Wagner, M.; Zhang, L.; Zhao, Z.; Thiemens, M.; Dominguez, G.; et al. Gate-tuning of graphene plasmons revealed by infrared nano-imaging. *Nature* **2012**, *487* (7405), 82−85.

(10) Ni, G.; McLeod, d. A.; Sun, Z.; Wang, L.; Xiong, L.; Post, K.; Sunku, S.; Jiang, B.-Y.; Hone, J.; Dean, C. R.; et al. Fundamental limits to graphene plasmonics. *Nature* **2018**, *557* (7706), 530−533.

(11) Low, T.; Roldán, R.; Wang, H.; Xia, F.; Avouris, P.; Moreno, L. M.; Guinea, F. Plasmons and screening in monolayer and multilayer black phosphorus. *Phys. Rev. Lett.* **2014**, *113* (10), 106802.

(12) Huber, M. A.; Mooshammer, F.; Plankl, M.; Viti, L.; Sandner, F.; Kastner, L. Z.; Frank, T.; Fabian, J.; Vitiello, M. S.; Cocker, T. L. Femtosecond photo-switching of interface polaritons in black phosphorus heterostructures. *Nat. Nanotechnol.* **2017**, *12* (3), 207−211.

(13) Dai, S.; Fei, Z.; Ma, Q.; Rodin, A.; Wagner, M.; McLeod, A.; Liu, M.; Gannett, W.; Regan, W.; Watanabe, K.; et al. Tunable phonon polaritons in atomically thin van der Waals crystals of boron nitride. *Science* **2014**, *343* (6175), 1125−1129.

(14) Caldwell, J. D.; Kretinin, A. V.; Chen, Y.; Giannini, V.; Fogler, M. M.; Francescato, Y.; Ellis, C. T.; Tischler, J. G.; Woods, C. R.; Giles, A. J.; et al. Sub-diffractional volume-confined polaritons in the natural hyperbolic material hexagonal boron nitride. *Nat. Commun.* **2014**, *5* (1), 1−9.

(15) Caldwell, J. D.; Aharonovich, I.; Cassabois, G.; Edgar, J. H.; Gil, B.; Basov, D. Photonics with hexagonal boron nitride. *Nat. Rev. Mater.* **2019**, *4* (8), 552−567.

(16) Ma, W.; Alonso-González, P.; Li, S.; Nikitin, A. Y.; Yuan, J.; Martín-Sánchez, J.; Taboada-Gutiérrez, J.; Amenabar, I.; Li, P.; Vélez, S.; et al. In-plane anisotropic and ultra-low-loss polaritons in a natural van der Waals crystal. *Nature* **2018**, *562* (7728), 557−562.

(17) Zheng, Z.; Xu, N.; Oscurato, S. L.; Tamagnone, M.; Sun, F.; Jiang, Y.; Ke, Y.; Chen, J.; Huang, W.; Wilson, W. L.; et al. A mid-infrared biaxial hyperbolic van der Waals crystal. *Sci. Adv.* **2019**, *5* (5), eaav8690.

(18) Zheng, Z.; Chen, J.; Wang, Y.; Wang, X.; Chen, X.; Liu, P.; Xu, J.; Xie, W.; Chen, H.; Deng, S.; et al. Highly confined and tunable hyperbolic phonon polaritons in van der Waals semiconducting transition metal oxides. *Adv. Mater.* **2018**, *30* (13), 1705318.

(19) Dai, Z.; Hu, G.; Si, G.; Ou, Q.; Zhang, Q.; Balendhran, S.; Rahman, F.; Zhang, B. Y.; Ou, J. Z.; Li, G.; et al. Edge-oriented and steerable hyperbolic polaritons in anisotropic van der Waals nanocavities. *Nat. Commun.* **2020**, *11* (1), 1−8.

(20) Fei, Z.; Scott, M.; Gosztola, D.; Foley, J., IV; Yan, J.; Mandrus, D.; Wen, H.; Zhou, P.; Zhang, D.; Sun, Y.; et al. Nano-optical imaging of WSe_2 waveguide modes revealing light-exciton interactions. *Phys. Rev. B* **2016**, *94* (8), 081402.

(21) Qi, P.; Luo, Y.; Shi, B.; Li, W.; Liu, D.; Zheng, L.; Liu, Z.; Hou, Y.; Fang, Z. Phonon scattering and exciton localization: molding exciton flux in two dimensional disorder energy landscape. *eLight* **2021**, *1* (1), 1−12.

(22) Liu, X.; Galfsky, T.; Sun, Z.; Xia, F.; Lin, E.-c.; Lee, Y.-H.; Kéna-Cohen, S.; Menon, V. M. Strong light−matter coupling in two-dimensional atomic crystals. *Nat. Photonics* **2015**, *9* (1), 30−34.

(23) Nemilentsau, A.; Low, T.; Hanson, G. Anisotropic 2D materials for tunable hyperbolic plasmonics. *Phys. Rev. Lett.* **2016**, *116* (6), 066804.

(24) Ma, W.; Shabbir, B.; Ou, Q.; Dong, Y.; Chen, H.; Li, P.; Zhang, X.; Lu, Y.; Bao, Q. Anisotropic polaritons in van der Waals materials. *InfoMat* **2020**, *2* (5), 777−790.

(25) Hu, G.; Shen, J.; Qiu, C. W.; Alù, A.; Dai, S. Phonon polaritons and hyperbolic response in van der Waals materials. *Adv. Opt. Mater.* **2020**, *8* (5), 1901393.

(26) Lee, D.; So, S.; Hu, G.; Kim, M.; Badloe, T.; Cho, H.; Kim, J.; Kim, H.; Qiu, C.-W.; Rho, J. Hyperbolic metamaterials: fusing artificial structures to natural 2D materials. *eLight* **2022**, *2* (1), 1−23.

(27) Krishnamoorthy, H. N.; Jacob, Z.; Narimanov, E.; Kretzschmar, I.; Menon, V. M. Topological transitions in metamaterials. *Science* **2012**, *336* (6078), 205−209.

(28) Li, P.; Hu, G.; Dolado, I.; Tymchenko, M.; Qiu, C.-W.; Alfaro-Mozaz, F. J.; Casanova, F.; Hueso, L. E.; Liu, S.; Edgar, J. H.; et al.

https://doi.org/10.1021/acs.nanolett.2c00399
Nano Lett. XXXX, XXX, XXX−XXX

Collective near-field coupling and nonlocal phenomena in infrared-phononic metasurfaces for nano-light canalization. *Nat. Commun.* **2020**, *11* (1), 1−8.
(29) Zhang, Q.; Hu, G.; Ma, W.; Li, P.; Krasnok, A.; Hillenbrand, R.; Alù, A.; Qiu, C.-W. Interface nano-optics with van der Waals polaritons. *Nature* **2021**, *597* (7875), 187−195.
(30) Gomez-Diaz, J. S.; Tymchenko, M.; Alu, A. Hyperbolic plasmons and topological transitions over uniaxial metasurfaces. *Phys. Rev. Lett.* **2015**, *114* (23), 233901.
(31) Gomez-Diaz, J.; Alu, A. Flatland optics with hyperbolic metasurfaces. *ACS Photonics* **2016**, *3* (12), 2211−2224.
(32) Li, P.; Dolado, I.; Alfaro-Mozaz, F. J.; Casanova, F.; Hueso, L. E.; Liu, S.; Edgar, J. H.; Nikitin, A. Y.; Vélez, S.; Hillenbrand, R. Infrared hyperbolic metasurface based on nanostructured van der Waals materials. *Science* **2018**, *359* (6378), 892−896.
(33) Hu, G.; Krasnok, A.; Mazor, Y.; Qiu, C.-W.; Alù, A. Moiré hyperbolic metasurfaces. *Nano Lett.* **2020**, *20* (5), 3217−3224.
(34) Hu, G.; Ou, Q.; Si, G.; Wu, Y.; Wu, J.; Dai, Z.; Krasnok, A.; Mazor, Y.; Zhang, Q.; Bao, Q.; et al. Topological polaritons and photonic magic angles in twisted α-MoO_3 bilayers. *Nature* **2020**, *582* (7811), 209−213.
(35) Zheng, Z.; Sun, F.; Huang, W.; Jiang, J.; Zhan, R.; Ke, Y.; Chen, H.; Deng, S. Phonon polaritons in twisted double-layers of hyperbolic van der Waals crystals. *Nano Lett.* **2020**, *20* (7), 5301−5308.
(36) Duan, J.; Capote-Robayna, N.; Taboada-Gutiérrez, J.; Álvarez-Pérez, G.; Prieto, I.; Martín-Sánchez, J.; Nikitin, A. Y.; Alonso-González, P. Twisted nano-optics: Manipulating light at the nanoscale with twisted phonon polaritonic slabs. *Nano Lett.* **2020**, *20* (7), 5323−5329.
(37) Chen, M.; Lin, X.; Dinh, T. H.; Zheng, Z.; Shen, J.; Ma, Q.; Chen, H.; Jarillo-Herrero, P.; Dai, S. Configurable phonon polaritons in twisted α-MoO_3. *Nat. Mater.* **2020**, *19* (12), 1307−1311.
(38) Chaudhary, K.; Tamagnone, M.; Rezaee, M.; Bediako, D. K.; Ambrosio, A.; Kim, P.; Capasso, F. Engineering phonon polaritons in van der Waals heterostructures to enhance in-plane optical anisotropy. *Sci. Adv.* **2019**, *5* (4), eaau7171.
(39) Zhang, Q.; Ou, Q.; Hu, G.; Liu, J.; Dai, Z.; Fuhrer, M. S.; Bao, Q.; Qiu, C.-W. Hybridized hyperbolic surface phonon polaritons at α-MoO_3 and polar dielectric interfaces. *Nano Lett.* **2021**, *21* (7), 3112−3119.
(40) Duan, J.; Álvarez-Pérez, G.; Voronin, K. V.; Prieto, I.; Taboada-Gutiérrez, J.; Volkov, V. S.; Martín-Sánchez, J.; Nikitin, A. Y.; Alonso-González, P. Enabling propagation of anisotropic polaritons along forbidden directions via a topological transition. *Sci. Adv.* **2021**, *7* (14), eabf2690.
(41) Fei, Z.; Rodin, A.; Gannett, W.; Dai, S.; Regan, W.; Wagner, M.; Liu, M.; McLeod, A.; Dominguez, G.; Thiemens, M.; et al. Electronic and plasmonic phenomena at graphene grain boundaries. *Nat. Nanotechnol.* **2013**, *8* (11), 821−825.
(42) Wu, Y.; Ou, Q.; Yin, Y.; Li, Y.; Ma, W.; Yu, W.; Liu, G.; Cui, X.; Bao, X.; Duan, J.; et al. Chemical switching of low-loss phonon polaritons in α-MoO_3 by hydrogen intercalation. *Nat. Commun.* **2020**, *11* (1), 1−8.
(43) Wu, Y.; Ou, Q.; Dong, S.; Hu, G.; Si, G.; Dai, Z.; Qiu, C. W.; Fuhrer, M. S.; Mokkapati, S.; Bao, Q. Efficient and Tunable Reflection of Phonon Polaritons at Built-In Intercalation Interfaces. *Adv. Mater.* **2021**, *33*, 2008070.
(44) Yang, X.; Zhai, F.; Hu, H.; Hu, D.; Liu, R.; Zhang, S.; Sun, M.; Sun, Z.; Chen, J.; Dai, Q. Far-Field Spectroscopy and Near-Field Optical Imaging of Coupled Plasmon−Phonon Polaritons in 2D van der Waals Heterostructures. *Adv. Mater.* **2016**, *28* (15), 2931−2938.
(45) Álvarez-Pérez, G.; González-Morán, A.; Capote-Robayna, N.; Voronin, K. V.; Duan, J.; Volkov, V. S.; Alonso-González, P.; Nikitin, A. Y. Active tuning of highly anisotropic phonon polaritons in van der Waals crystal slabs by gated graphene. *ACS Photonics* **2022**, *9* (2), 383−390.
(46) Hu, H.; Chen, N.; Teng, H.; Yu, R.; Qu, Y.; Sun, J.; Xue, M.; Hu, D.; Wu, B.; Li, C., Doping-driven topological polaritons in graphene/α-MoO_3 heterostructures. *arXiv preprint arXiv:2201.00930* 4 Jan 2022. DOI: 10.48550/arXiv.2201.00930 (accessed 2022-04-03).
(47) Bapat, A.; Dixit, S.; Gupta, Y.; Kumar, A., Gate tunable light-matter interaction in natural biaxial hyperbolic van der Waals heterostructures. *arXiv preprint arXiv:2110.07526* 14 Oct 2021. DOI: 10.48550/arXiv.2110.07526 (accessed 2022-04-03).

https://doi.org/10.1021/acs.nanolett.2c00399
Nano Lett. XXXX, XXX, XXX−XXX